

Nanoscale

Accepted Manuscript

This article can be cited before page numbers have been issued, to do this please use: G. Raj, T. Ghosh, V. D. S., H. P., D. B. Kumar, J. Prasad, V. B. Athul, A. S. M and R. Varghese, *Nanoscale*, 2024, DOI: 10.1039/D4NR01494D.



This is an Accepted Manuscript, which has been through the Royal Society of Chemistry peer review process and has been accepted for publication.

Accepted Manuscripts are published online shortly after acceptance, before technical editing, formatting and proof reading. Using this free service, authors can make their results available to the community, in citable form, before we publish the edited article. We will replace this Accepted Manuscript with the edited and formatted Advance Article as soon as it is available.

You can find more information about Accepted Manuscripts in the [Information for Authors](#).

Please note that technical editing may introduce minor changes to the text and/or graphics, which may alter content. The journal's standard [Terms & Conditions](#) and the [Ethical guidelines](#) still apply. In no event shall the Royal Society of Chemistry be held responsible for any errors or omissions in this Accepted Manuscript or any consequences arising from the use of any information it contains.

ARTICLE

G₄-Hemin loaded 2D nanosheets for combined and targeted chemo-photodynamic cancer therapyGowtham Raj,^a Tamraparni Ghosh,^a Vasudev D. S.,^a Harsha P.,^a Devu B. Kumar,^b Justin Prasad,^a Athul V. B.,^b Abhimanyu S. M.,^b and Reji Varghese^{*a}Received 00th January 20xx,
Accepted 00th January 20xx

DOI: 10.1039/x0xx00000x

Synergetic combination therapy is emerging as one of the most promising approaches for cancer treatment. Among the various therapeutic approaches, PDT has received particular attention due to its non-invasive nature. However, therapeutic performance of PDT is severely affected by tumour hypoxia. Herein, we report a supramolecular strategy for the fabrication of a PDT active 2D nanosheet loaded with a POD mimicking DNAzyme for the synergetic combination of PDT and CDT for targeted cancer therapy. Assembly of biotin functionalized BODIPY (**1**) and cationic β -cyclodextrin (β -CD⁺) leads to the formation of **1/** β -CD⁺ nanosheet with positively charged β -CD⁺ on the surface of the sheet. The cationic face of **1/** β -CD⁺ sheet was then loaded with POD-mimicking Hemin-loaded G-quadruplex aptamer (**Hem/DNA1**) via electrostatic interaction (**1/** β -CD⁺/**Hem/DNA1**). Cellular internalization of **1/** β -CD⁺/**Hem/DNA1** nanosheet occurs via receptor-mediated endocytic pathway, which then undergoes lysosomal escape. Subsequently, **Hem/DNA1** on the surface of **1/** β -CD⁺/**Hem/DNA1** reacts with endogenous H₂O₂ via the Fenton pathway produces [•]OH and O₂. Moreover, under cellular conditions, **Hem** inside **1/** β -CD⁺/**Hem/DNA1** nanosheet produces Fe²⁺, which then undergoes another Fenton reaction to produce [•]OH and O₂. The Fe³⁺ generated after Fenton reaction then in-situ get reduced to Fe²⁺ by glutathione for the next Fenton cycle. At the same time, photoirradiation of **1/** β -CD⁺ nanosheet using 635 nm laser produces ¹O₂ via PDT pathway by using the endogenous O₂. The most remarkable feature of the present nanoformulation is the cooperativity in its therapeutic action, wherein O₂ produced during CDT pathway was used by **1/** β -CD⁺ sheet for improving its PDT efficacy in the hypoxic tumor microenvironment. This work represents a unique combination of CDT and PDT for targeted cancer therapy, wherein, CDT action of the nanoagent enhances the PDT efficacy and we strongly believe that this approach would encourage researchers to design similar combination therapy for the advancements in the treatment of cancer.

Introduction

Photodynamic therapy (PDT) is a promising treatment modality for cancer mainly due to its non-invasive nature and spatiotemporal controllability.^{1,2} It involves the photoexcitation of a photosensitizer, preferably in the near-infrared (NIR) region, which then undergoes intersystem crossing from the singlet excited state to the triplet excited state. The triplet state of the sensitizer then acts as an energy donor to the ground state of molecular oxygen (³O₂) and other molecules present in the tissue, producing highly cytotoxic reactive oxygen species (ROS) including singlet oxygen (¹O₂). These reactions lead to cell death at the photoirradiated region.^{3–9} Although considerable advancement has been made in PDT-based cancer treatment, the condition of hypoxia (reduced oxygen concentration) in solid tumours significantly reduces the efficiency of PDT for cancer treatment.^{10,11} Different strategies have been developed in recent years to

overcome the tumour hypoxia condition such as by transporting additional O₂ to the tumor microenvironment^{12,13} and by catalysing endogenous H₂O₂ to O₂.^{14,15} Though these strategies showed enhanced supply of O₂ to the hypoxic tumours to some extent, the continuous consumption of O₂ by the mitochondria for the synthesis of ATP significantly hinders the efficacy of these approaches. Therefore, development of new strategies to boost O₂ concentration in hypoxic tumours is extremely important for PDT-based cancer therapy.^{16–18}

Chemodynamic therapy (CDT) is another potential therapeutic approach for cancer treatment and has shown significant growth in recent years.^{19,20} This involves the metal catalysed conversion of endogenous H₂O₂ into highly reactive hydroxyl radicals ([•]OH) via a Fenton or Fenton-like reaction.^{21,22} It is important to note that one of the by-products of Fenton reaction is O₂. This clearly suggest that the integration of a CDT agent with the PDT system would be a promising approach for the improvement of PDT action by boosting the concentration of O₂. More importantly, CDT and PDT can work in a synergetic fashion wherein O₂ generated by Fenton reaction can enhance the PDT action and at the same time [•]OH generated via Fenton reaction is toxic to the cancer cells. Hence, this strategy offer the design of synergetic combination of PDT and CDT for the treatment of cancer.^{23–28}

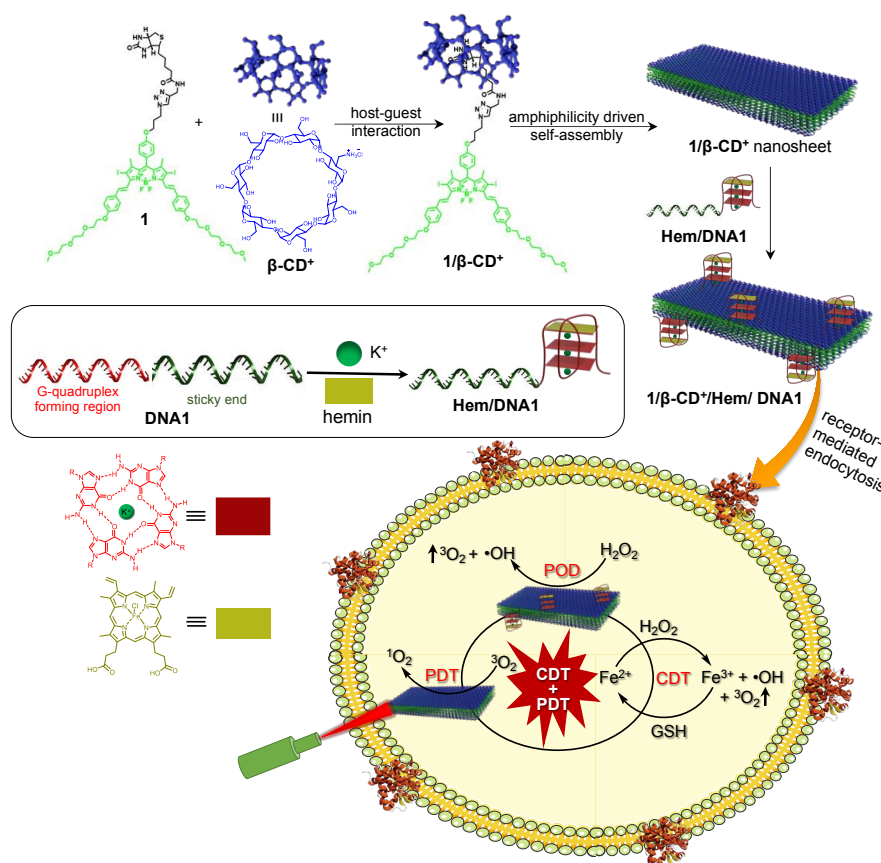
^aSchool of Chemistry, Indian Institute of Science Education and Research (IISER) Thiruvananthapuram, Trivandrum-695551, Kerala, India.

Email: reji@iisertvm.ac.in

^bSchool of Biology, Indian Institute of Science Education and Research (IISER) Thiruvananthapuram, Trivandrum-695551, Kerala, India.

Electronic Supplementary Information (ESI) available: [details of any supplementary information available should be included here]. See DOI: 10.1039/x0xx00000x





Scheme 1. Scheme showing the non-covalent synthesis of $1/\beta\text{-CD}^+$ complex and its spontaneous self-assembly to the formation of $1/\beta\text{-CD}^+$ nanosheet. Integration of **Hem/DNA1** onto the surface of $1/\beta\text{-CD}^+$ nanosheet via electrostatic interactions is also shown. Cellular internalization of $1/\beta\text{-CD}^+/\text{Hem/DNA1}$ into MDA-MB-231 cells through receptor mediated endocytosis and the mechanism of combined PDT and CDT are also demonstrated.

We have recently reported a fluorinated boron-dipyromethene (BODIPY)-based nanosheet as a nanoformulation for combined antisense DNA delivery and PDT.²⁹ The nanosheet exhibited high extinction coefficient in the NIR region, excellent $^1\text{O}_2$ generation upon photoirradiation and efficient delivery of antisense DNA.^{30,31} Because the surface of the nanosheet is cationic in nature, it permits the integration of any functional DNA onto its surface via electrostatic interaction. In view of this, we envisioned that the incorporation of a peroxidase (POD)-mimicking DNAzyme³²⁻³⁵ onto PDT active nanosheet would be a promising nanoformulation to achieve the design of synergetic combination of CDT and PDT.³⁶⁻³⁸ For example, G-rich DNA is known to fold G-quadruplexes that show high binding affinity to hemin (**Hem**) to form **Hem**-bound G-quadruplex, which is known to exhibit POD activity to produce $\cdot\text{OH}$ and O_2 .³⁹ In addition, G-quadruplex can function as an aptamer for specific cancer cell and hence offer targeted delivery of therapeutic agents into cancerous cells.^{40,41}

Herein, we report a supramolecular strategy for the fabrication of a PDT active 2D nanosheet loaded with a POD-mimicking DNAzyme for the synergetic combination of PDT and CDT-based cancer therapy. As reported previously, the host-guest interaction between biotin functionalized BODIPY (**1**) and cationic β -cyclodextrin ($\beta\text{-CD}^+$) in aqueous medium resulted in the formation of $1/\beta\text{-CD}^+$ nanosheet with positively charged $\beta\text{-CD}^+$ exposed onto the surface of the sheet.²⁹ The cationic faces

of $1/\beta\text{-CD}^+$ were then loaded with POD-mimicking **Hem**-loaded G-quadruplex aptamer (**Hem/DNA1**) via electrostatic interaction to form $1/\beta\text{-CD}^+/\text{Hem/DNA1}$ nanosheet. Importantly, **DNA1** (DNAzyme) on the surface of the nanosheet can act as a targeting ligand for the overexpressed nucleolin protein on the surface of cancer cells (eg.: MDA-MB-231) for the selective delivery of PDT and CDT agents.⁴²⁻⁴⁴ After selective cellular internalization of $1/\beta\text{-CD}^+/\text{Hem/DNA1}$ nanosheet via receptor-mediated endocytic pathway, it undergoes lysosomal escape due to the cationic charge on the surface of the nanosheet, which potentially prevents its degradation at the lysosome. Subsequently, **Hem/DNA1** on the surface of $1/\beta\text{-CD}^+/\text{Hem/DNA1}$ reacts with endogenous H_2O_2 via the Fenton pathway produces $\cdot\text{OH}$ and O_2 . Moreover, under cellular conditions, over time, **Hem** inside $1/\beta\text{-CD}^+/\text{Hem/DNA1}$ nanosheet produces Fe^{2+} by the enzymatic action of intracellular heme oxygenase.⁴⁵ The in-situ generated Fe^{2+} then undergoes another Fenton reaction to produce $\cdot\text{OH}$ and O_2 . The Fe^{3+} generated after Fenton reaction then in-situ get reduced to Fe^{2+} by glutathione (GSH) for the next Fenton cycle. At the same time, photoirradiation of $1/\beta\text{-CD}^+$ nanosheet using 635 nm laser produces $^1\text{O}_2$ via PDT by using endogenous O_2 . The most remarkable feature of the nanoformulation is the cooperativity in its therapeutic action, wherein O_2 produced during CDT pathway was used by $1/\beta\text{-CD}^+$ sheet for improving its PDT efficacy in the hypoxic tumor microenvironment (Scheme 1).



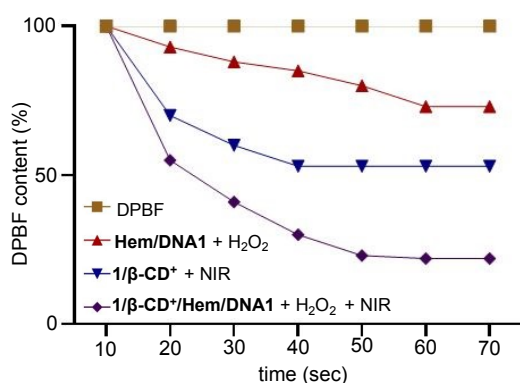


Figure 2. Plot of absorbance changes of DPBF at 420 nm of DPBF-treated solutions of Hem/DNA1, 1/β-CD⁺ and 1/β-CD⁺/Hem/DNA1 under photoirradiation with 635 nm laser for 70 sec (0.75 W/cm²).

Hem/DNA1 as evident from the transmission electron (TEM) (Figure 1e) and atomic force microscopic (AFM) (Figure 1f) analyses. Nanosheet morphology of 1/β-CD⁺/Hem/DNA1 was further confirmed by confocal laser scanning microscopic (CLSM) analyses using DNA1 labelled with FAM (DNA2), which showed the formation of green fluorescent 2D nanosheets (Figure 1g). Furthermore, 1/β-CD⁺/Hem/DNA1 nanosheet was found to be structurally stable in PBS buffer and 10 % serum at pH 7.0. This was evident from the time-dependent absorption spectral changes of 1/β-CD⁺/Hem/DNA1 nanosheet, which revealed no change in the characteristic absorption of the nanosheet with respect to time, at least up to 6 h (Figure S3). We also evaluated whether the POD-mimicking activity of Hem/DNA1 retains after loading onto the nanosheet. As

expected, a strong absorption peak at 650 nm was observed for 1/β-CD⁺/Hem/DNA1-treated samples, validating its catalytic activity even after loading onto the nanosheet (Figure 1c).

One of the by-products of CDT action of Hem/DNA1 is O₂ and hence the in-situ generated O₂ can be utilized by the photosensitizer (1/β-CD⁺) for the enhanced generation of ¹O₂ under the hypoxic conditions of tumour microenvironment. The CDT-assisted enhanced PDT of 1/β-CD⁺/Hem/DNA1 was studied using 1,3-diphenylisobenzofuran (DPBF) degradation assay. For this, Hem/DNA1 (1/1 μM) and 1/β-CD⁺/Hem/DNA1 (50/50/1/1 μM) nanosheets solutions in water (pH 6.5) containing H₂O₂ (200 μM) and DPBF (200 μM) was irradiated with a 635 nm laser (0.75 W/cm²) for 70 sec and the decrease in the absorption band of DPBF at 420 nm was monitored with respect to time (Figure 2). Absorption spectrum of DPBF was considered as the control (100 %) and no degradation was observed in this case. A decrease of 27 % in the absorption of DPBF was observed for Hem/DNA1-treated sample compared to DPBF alone, indicating the degradation of DPBF by the in-situ generated [•]OH by the CDT action of Hem/DNA1. Interestingly, a drastic decrease of 73 % in DPBF absorption was observed for 1/β-CD⁺/Hem/DNA1-treated sample. This enhanced degradation of DPBF in the case of 1/β-CD⁺/Hem/DNA1 compared to Hem/DNA1 must be attributed to the synergetic action of CDT and PDT, wherein O₂ generated during the CDT action of Hem/DNA1 enhances the PDT action of 1/β-CD⁺.

Having demonstrated the synergetic action of CDT and PDT, the therapeutic performance of 1/β-CD⁺/Hem/DNA1 nanosheet for combined CDT and PDT-based cancer therapy

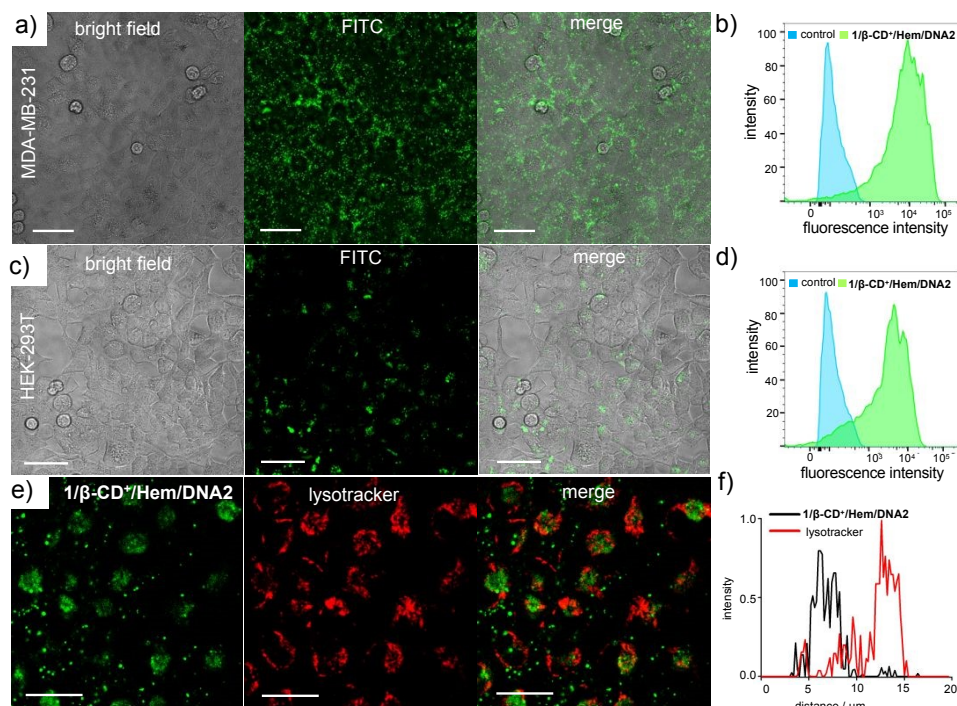


Figure 3. (a) CLSM images of 1/β-CD⁺/Hem/DNA2-treated MDA-MB-231 cells (scale bar represents 50 μm) and (b) the corresponding FACS analyses. (c) CLSM images of 1/β-CD⁺/Hem/DNA2-treated HEK-293T cells (scale bar represents 50 μm) and (d) the corresponding FACS analyses. (e) CLSM images of 1/β-CD⁺/Hem/DNA2-treated MDA-MB-231 cells stained with lysotracker red (scale bar represents 25 μm) and (f) the corresponding line analyses.



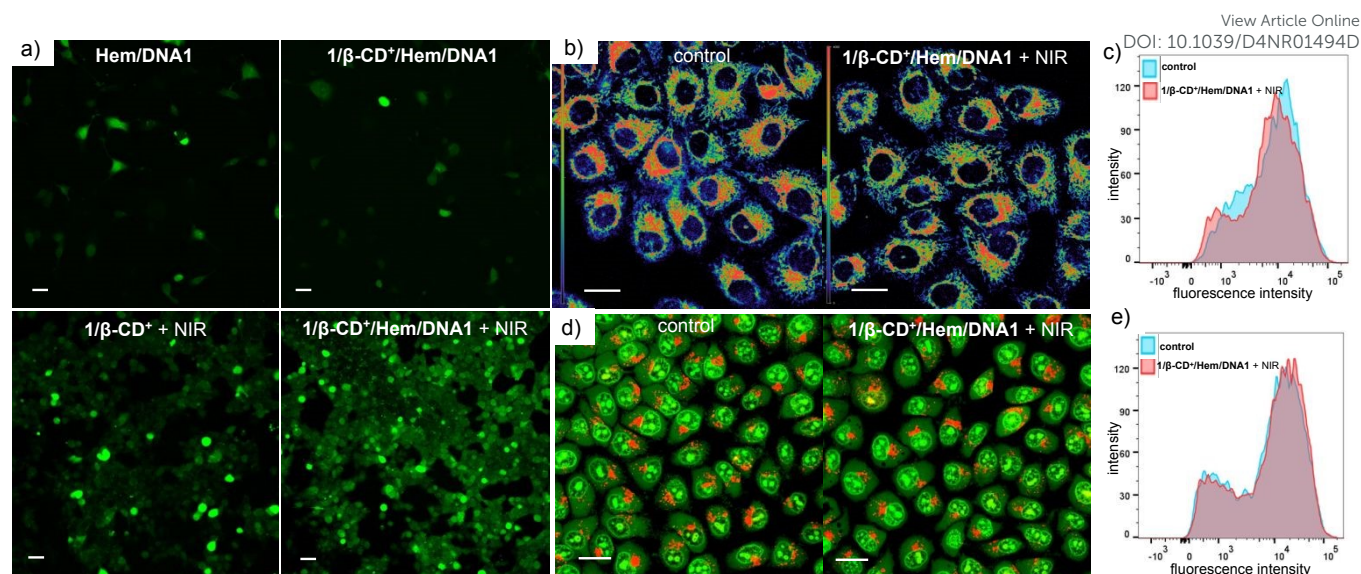


Figure 4. (a) DCFH-DA assay: CLSM images of Hem/DNA1, 1/β-CD⁺/Hem/DNA1, 1/β-CD⁺ + NIR and 1/β-CD⁺/Hem/DNA1 + NIR-treated MDA-MB-231 cells (635 nm laser with power of 0.75 W/cm²) (scale bar represents 25 μm). (b) TMRM assay: CLSM images of 1/β-CD⁺/Hem/DNA1-treated MDA-MB-231 cells stained with TMRM under photoirradiation at 635 nm laser (0.75 W/cm²) (scale bar represents 25 μm) and (c) the corresponding FACS analyses. (d) AO assay: CLSM images of 1/β-CD⁺/Hem/DNA1-treated MDA-MB-231 cells stained with AO under photoirradiation at 635 nm laser (0.75 W/cm²) (scale bar represents 25 μm) and (e) the corresponding FACS analyses.

was studied using triple-negative human breast cancer cells, MDA-MB-231, as a representative cell line. Initially, the cellular internalization of 1/β-CD⁺/Hem/DNA2 (20/20/1/1 μM) was investigated using CLSM analyses by monitoring the green fluorescence of DNA2. After 12 h of incubation, CLSM analyses revealed strong green fluorescence for the cells and was mainly distributed through the cytosolic regions of the cells (Figure 3a and b). This indicates the efficient internalization of 1/β-CD⁺/Hem/DNA2 into MDA-MB-231 cells. It is important to note that Hem/DNA1 not only acts as a CDT agent, but also acts as a targeting ligand for MDA-MB-231 cells. Targeting of the cancer cells was due to the molecular recognition of nucleolin protein overexpressed on the surface of MDA-MB-231 cells by Hem/DNA2. Thereby, Hem/DNA2 permits the selective internalization of the nanoformulation into the cancer cells preferably compared to the normal healthy cell lines. The selective internalization of 1/β-CD⁺/Hem/DNA2 was evaluated by comparing its cellular internalization between HEK-293T (normal cell line), which has negligible expression of nucleolin on its surface, and MDA-MB-231 cancer cells (Figure 3a–d). In accordance with our design, CLSM analyses clearly showed strong green fluorescence for 1/β-CD⁺/Hem/DNA2-treated MDA-MB-231 cells (Figure 3a and b) when compared to the corresponding HEK-293T cells (Figure 3c and d). In support of this, fluorescence-activated cell sorting (FACS) analyses revealed high mean fluorescence intensity (MFI) shift for MDA-MB-231 (11490) compared to HEK-293T cells (4440).

Typically any foreign materials entering into a cell via endocytic pathway ultimately reaches at the lysosome and get degraded at the lysosome due to its acidic pH. In order to check whether the nanosheet reaches at the lysosome after its cellular internalization, colocalization studies were performed after staining the lysosome of the cells using lysotracker red (Figure 3e). As evident from the CLSM analyses that only very poor

colocalization was observed for 1/β-CD⁺/Hem/DNA2 nanosheet with lysotracker deep red. This suggests that 1/β-CD⁺/Hem/DNA2 nanosheet undergoes lysosomal escape immediately after the receptor-mediated endocytosis and escape the degradation at the lysosome. This was further supported by the corresponding line analyses, which showed a relatively low Pearson Coefficient value of 0.048 (Figure 3f). We believe that the lysosomal escape of 1/β-CD⁺/Hem/DNA2 nanosheet is due to the net positive charges present on the surface of the nanosheet, which favours the lysosomal membrane destabilization, as reported previously by our own group and others.⁵⁰ The lysosomal escape of 1/β-CD⁺/Hem/DNA2 prevents the degradation of the nanosheet at the acidic lysosomes and thereby improving the efficacy of the nanoformulation.

After establishing the escape of 1/β-CD⁺/Hem/DNA2 nanosheet from the lysosomes, the ROS generation efficiency of 1/β-CD⁺/Hem/DNA1 nanosheet inside MDA-MB-231 cell was investigated using 2',7'-dichlorofluorescein diacetate (DCFH-DA) as a fluorescent probe for ROS. For this, MDA-MB-231 cells were treated with Hem/DNA1, 1/β-CD⁺/Hem/DNA1, 1/β-CD⁺ + NIR or 1/β-CD⁺/Hem/DNA1 + NIR (635 nm laser with a power of 0.75 W/cm² for 10 minutes) and the in-situ ROS generation inside the cell was monitored by DCFH-DA assay, which produces green fluorescent 2,7-dichlorofluorescein (DCF) upon ROS detection (Figure 4a). CLSM analyses clearly revealed that maximum green fluorescence intensity of DCF was associated with 1/β-CD⁺/Hem/DNA1 + NIR-treated cells compared to Hem/DNA1, 1/β-CD⁺/Hem/DNA1, 1/β-CD⁺ + NIR-treated cells. These results unequivocally confirm that 1/β-CD⁺/Hem/DNA1 + NIR-treated cells produces maximum ROS inside the cells upon laser irradiation and this must be attributed to the synergistic action of CDT and PDT. In accordance with the CLSM, FACS analyses disclosed MFI shift values of 6052, 1240, 463 and 127



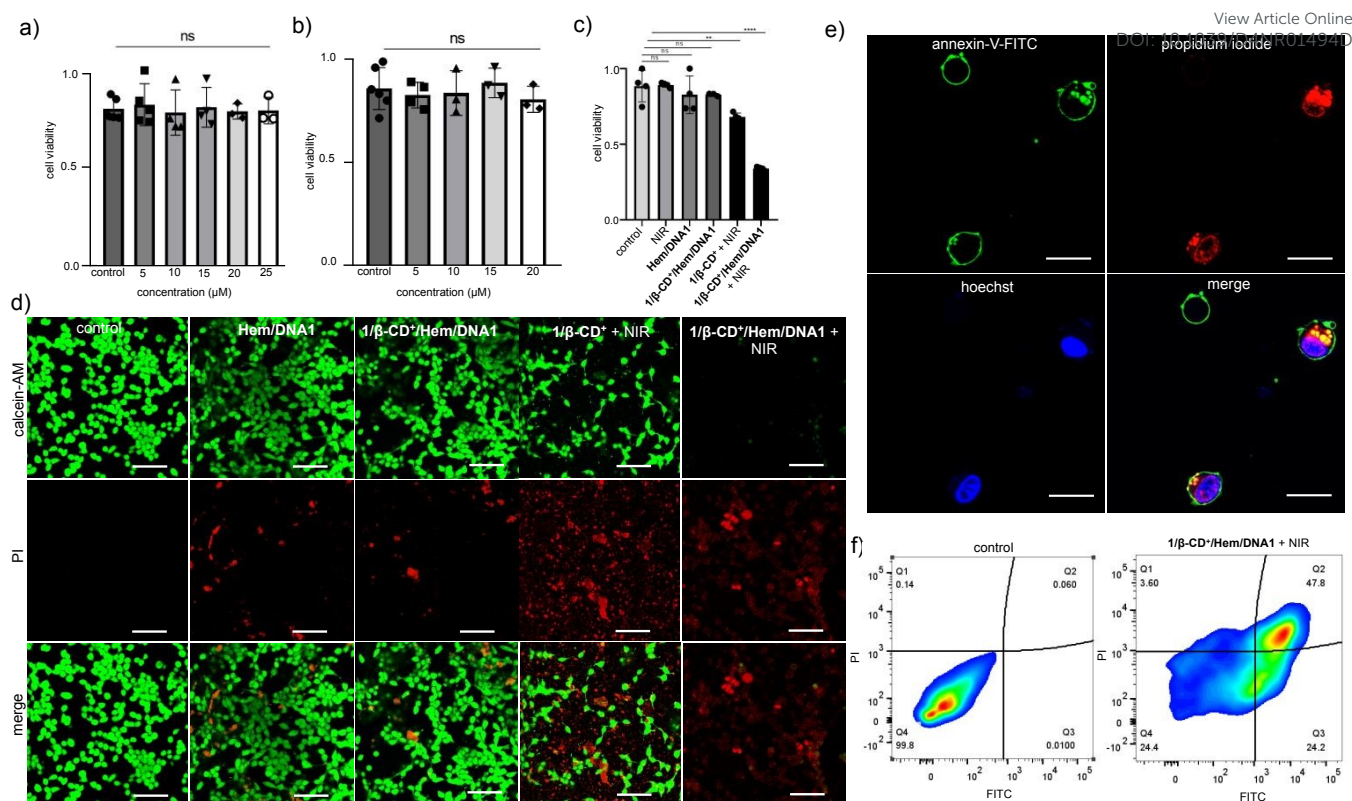


Figure 5. (a)–(c) MTT assay: cell viability at varying concentrations of (a) β -CD* and (b) $1/\beta$ -CD*-treated MDA-MB-231 cells in the dark. (c) MTT assay for Hem/DNA1, $1/\beta$ -CD*/Hem/DNA1, $1/\beta$ -CD* + NIR and $1/\beta$ -CD*/Hem/DNA1 + NIR-treated MDA-MB-231 cells (635 nm laser with a power of 0.75 W/cm²). (d) Calcein-AM/PI live-dead assay: CLSM images of Hem/DNA1, $1/\beta$ -CD*/Hem/DNA1, $1/\beta$ -CD* + NIR and $1/\beta$ -CD*/Hem/DNA1 + NIR-treated MDA-MB-231 cells (scale bar represents 100 μ m). (e) Annexin V-FITC/PI assay: CLSM images of $1/\beta$ -CD*/Hem/DNA1-treated MDA-MB-231 cells under photoirradiation using 635 nm laser (0.75 W/cm²) (scale bar represents 25 μ m) and (f) the corresponding FACS analyses.

for $1/\beta$ -CD*/Hem/DNA1 + NIR, $1/\beta$ -CD*, Hem/DNA1 and untreated MDA-MB-231 cells, respectively (Figure S5). Maximum MFI shift was observed for $1/\beta$ -CD*/Hem/DNA1 + NIR-treated cells. As expected, no significant ROS generation was observed for $1/\beta$ -CD*/Hem/DNA1-treated cells in the absence of photoirradiation.

Because ROS species such as ¹O₂ and *OH are highly oxidizing in nature and induce damage to organelles like lysosomes and mitochondria, which can potentially leads to apoptosis by various signalling pathways. In view of this, we examined the structural integrity of these organelles in the presence of ROS species generated by the combined CDT and PDT. The mitochondrial damage caused by the ROS was evaluated using tetramethylrhodamine methyl ester perchlorate (TMRM) assay (Figure 4b and c).⁵¹ Since mitochondria have typical membrane potentials in the range of -180 mV, they can accumulate high concentrations of cationic dyes like TMRM. If mitochondria are damaged or depolarized, dye accumulation gradually decreases, which leads to the diminishing of its fluorescence intensity. For this, MDA-MB-231 cells were treated with $1/\beta$ -CD*/Hem/DNA1 (20/20/1/1 μ M) for 2 h, then kept under NIR light illumination (635 nm laser at 0.75 W/cm²) for 10 minutes followed by 3 h of incubation. Cells were then stained with TMRM, and changes in green fluorescence intensity of TMRM were probed using CLSM analyses. In this case as well, CLSM analyses of $1/\beta$ -CD*/Hem/DNA1-treated MDA-MB-231 cells

showed no decrease in the fluorescence intensity when compared to the corresponding control cells, indicating the healthy nature of the mitochondria (Figure 4b). This was further quantified by FACS analyses (Figure 4c), which disclosed similar MFI shift values for $1/\beta$ -CD*/Hem/DNA1 treated (12674) and the corresponding untreated control cells (12660). The lysosomal integrity was further evaluated using an acridine orange (AO) assay (Figure 4d and e).^{52,53} Acridine orange emits green fluorescence when bound to dsDNA in the nucleus and red fluorescence inside lysosome. If the lysosome is damaged, it leads to a decrease in the red fluorescence of AO. For this purpose, MDA-MB-231 cells were treated with $1/\beta$ -CD*/Hem/DNA1 (20/20/1/1 μ M) for 2 h followed by NIR light illumination for 10 minutes followed by 3 h incubation. Subsequently, the cells were co-stained with AO and evaluated using CLSM analyses. CLSM images $1/\beta$ -CD*/Hem/DNA1-treated cells showed no noticeable decrease in the red fluorescence of AO with respect to the control cells, indicating that the lysosomes were not damaged by ROS generated by $1/\beta$ -CD*/Hem/DNA1 nanosheet (Figure 4d). This was further confirmed by FACS analyses, which showed MFI shift values of 16476 and 17527 for the control and $1/\beta$ -CD*/Hem/DNA1 nanosheet-treated MDA-MB-231 cells, respectively (Figure 4e). However it must be noted that TMRM and AO staining assays revealed significant damage to lysosome and mitochondria after 24 h of incubation (Figure S6). These results conclude that



ROS cause damage to the cell organelles at a larger time scale of incubation, but are intact at smaller incubation time.

After demonstrating the selective internalization and ROS generation inside the cancer cells, the cytotoxicity of **1/β-CD⁺/Hem/DNA1** towards MDA-MB-231 cells was studied using MTT assay.⁵⁴ Initially, toxicities of **β-CD⁺** and **1/β-CD⁺** nanosheets towards MDA-MB-231 cells in the dark was studied (Figure 5a and b). For this, **β-CD⁺** (Figure 5a) and **1/β-CD⁺** (Figure 5b) nanosheets under dark of varying concentrations (1-20 μM) were treated with MDA-MB-231 cells for 24 h. As expected, no cytotoxicity was observed even at a higher concentration of 20 μM. Subsequently, cytotoxicity of MDA-MB-231 cells treated with **Hem/DNA1** (1/1 μM), **1/β-CD⁺/Hem/DNA1** (20/20/1/1 μM), **1/β-CD⁺** (20/20 μM) + NIR, and **1/β-CD⁺/Hem/DNA1** + NIR (20/20/1/1 μM) for 2 h (635 nm laser with a power of 0.75 W/cm² for 10 minutes) were studied (Figure 5c). As expected no significant cytotoxicity was observed for **Hem/DNA1** and **1/β-CD⁺/Hem/DNA1** in the absence of NIR light, indicating the poor therapeutic efficacy. On the other hand, significant cytotoxicity was observed for **1/β-CD⁺** and **1/β-CD⁺/Hem/DNA1**-treated cell under NIR light irradiation. Interestingly, enhanced cytotoxicity was observed for **1/β-CD⁺/Hem/DNA1**-treated cells compared to **1/β-CD⁺**-treated cells. A cell death of 65 % was observed for **1/β-CD⁺/Hem/DNA1**-treated cells, whereas, only 32 % cell death was observed for **1/β-CD⁺**-treated cells. These results are in full agreement with the enhanced ROS generation for **1/β-CD⁺/Hem/DNA1**-treated cells and fully support our hypothesis of synergetic CDT and PDT actions.

To further support the cytotoxicity induced by the combined actions of CDT and PDT by **1/β-CD⁺/Hem/DNA1** nanosheet towards MDA-MB-231 cells, calcein-AM/PI co-staining assay was performed (live/dead assay) (Figure 5d). Calcein-AM interacts with the esterase present inside the live cancer cells and produce green fluorescence from the cells due to the cleavage of the acetoxymethyl (AM) ester-protecting group of calcein-AM. On the other hand, no ester cleavage is possible inside the dead cell as the concentration of esterase is very minimal and hence no green fluorescence is expected for the dead cells. Similarly, propidium iodide (PI) cannot pass through the cell membrane of live cells, whereas it can stain the dead cell to give red fluorescence.⁴³ To demonstrate the live/dead assay, cells were initially treated with **Hem/DNA1**, **1/β-CD⁺/Hem/DNA1**, **1/β-CD⁺** + NIR, **1/β-CD⁺/Hem/DNA1** + NIR for 2 h (635 nm laser with a power of 0.75 W/cm² for 10 minutes). As shown in Figure 5d, **1/β-CD⁺/Hem/DNA1** + NIR -treated cells exhibited mainly red fluorescence of PI and negligible green fluorescence of calcein-AM compared to **Hem/DNA1**, **1/β-CD⁺/Hem/DNA1**, **1/β-CD⁺** + NIR-treated cells. These results conclude the enhanced cytotoxicity of **1/β-CD⁺/Hem/DNA1** + NIR compared to **1/β-CD⁺** + NIR, **Hem/DNA1** and **1/β-CD⁺/Hem/DNA1**. Live/dead assay also support our hypothesis of enhanced cytotoxicity for **1/β-CD⁺/Hem/DNA1** + NIR due to the synergetic combination of CDT and PDT.

In order to understand the cell death mechanism of the present nanoformulation, annexin V-FITC(AV)/PI staining assay was carried out on **1/β-CD⁺/Hem/DNA1**-treated MDA-MB-231

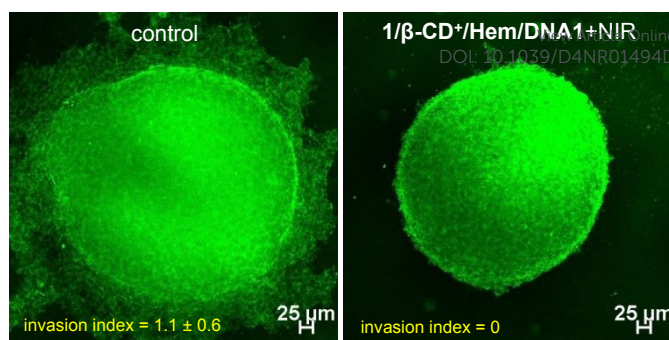


Figure 6. CLSM images of **1/β-CD⁺/Hem/DNA1**-treated MDA-MB-231 3D spheroids after NIR light illumination (0.75 W cm⁻² for 10 minutes) (right) and the corresponding untreated control spheroids (left).

cells under NIR light illumination. As shown in Figure 5e and Figure S7, **1/β-CD⁺/Hem/DNA1** (20/20/1/1 μM)-treated cells exhibited intense green fluorescence of annexin V-FITC around the cell membrane and strong red fluorescence of PI from the nuclei, revealing that the most of the cell population is in the late stage of apoptotic pathway. This is further confirmed through the FACS analyses (Figure 5f). For this purpose, MDA-MB-231 cells were treated with **1/β-CD⁺/Hem/DNA1** nanosheet under NIR light illumination and analysed by flow cytometry after staining with annexin V-FITC (AV)/PI. In accordance with the CLSM, the cell population mainly shifted to the quadrant corresponds to the apoptotic pathway. These results collectively conclude that **1/β-CD⁺/Hem/DNA1** nanosheet under NIR light illumination induces cell death via oxidative stress-induced apoptotic pathway.

After demonstrating the in vitro performance of **1/β-CD⁺/Hem/DNA1** nanosheet, we studied the efficiency of the nanoformulation in multicellular tumor spheroid model using 3D cell culture (Figure 6). The 3D-multicellular tumor spheroid mimics the in vivo tumor and they undergoes proliferation in all directions similar to malignant tumors. In 3D cell culture, cells clump together to form a stable 3D spheroid-like structure, wherein the communication and signalling between the cells are maximized, leading to efficient proliferation and invasion over time.⁵⁵ To this end, 3D tumour spheroids of MDA-MB-231 cells were prepared using the standard hanging drop method.^{56,57} The invasion potential of the 3D spheroids was studied in the presence of **1/β-CD⁺/Hem/DNA1** nanosheet after NIR light irradiation to understand its effect on the spheroid invasion. For this, 3D spheroids were incubated with **1/β-CD⁺/Hem/DNA1** (20/20/1/1 μM) nanosheet for 4 h, kept under irradiation at 635 nm (0.75 W/cm²) for 10 minutes followed by 24 h of incubation. Untreated spheroids were considered as controls that showed maximum invasion potential (invasion index = 1.1 ± 0.6) as they showed migration in all the directions. On the other hand, **1/β-CD⁺/Hem/DNA1**-treated sample showed drastic reduction in the invasion potential (invasion index = 0) of the spheroids due to the combined therapeutic actions of CDT and PDT. These observations are in good agreement with the in vitro studies.



Conclusions

In summary, we have reported a supramolecular strategy for the fabrication of a PDT active 2D nanosheet loaded with a POD-mimicking DNAzyme for the synergetic combination of PDT and CDT for targeted cancer therapy. The most important feature of the present nanoformulation is the synergetic combination of CDT and PDT actions. The CDT action of the nanoformulation results in the formation of highly toxic ROS along with the generation of O₂ as one of the bioproducts, which can boost the concentration of O₂ in the tumour microenvironment. This in turn enhance the PDT action of the nanoformulation, which is otherwise found to be less effective due to tissue hypoxia. Excellent therapeutic activity was demonstrated both in vitro and in vivo for targeted cancer therapy. This work represents a unique combination of CDT and PDT for targeted cancer therapy, wherein, CDT action of the nanoagent enhances the PDT efficacy and we strongly believe that this approach would encourage researchers to design similar combination therapy for the advancements in the treatment of cancer.

Author Contributions

The manuscript was written through the contributions of all authors. All authors have given approval to the final version of the manuscript.

Conflicts of interest

There are no conflicts to declare.

Acknowledgements

Financial support from SERB (CRG/2022/002612) is gratefully acknowledged. The help of Sarika Mohan S. is acknowledged for the FACS analyses.

References

- X. Zhao, J. Liu, J. Fan, H. Chao and X. Peng, *Chem. Soc. Rev.*, 2021, **50**, 4185–4219.
- T. C. Pham, V.-N. Nguyen, Y. Choi, S. Lee and J. Yoon, *Chem. Rev.* 2021, **121**, 13454–13619.
- S. S. Lucky, K. C. Soo and Y. Zhang, *Chem. Rev.* 2015, **115**, 1990–2042.
- K. Jibin, M. Victor, G. Saranya, H. Santhakumar, V. Murali, K. K. Maiti and R. S. Jayasree, *ACS Appl. Bio Mater.*, 2021, **4**, 5742–5752.
- H. He, P.-C. Lo, S.-L. Yeung, W.-P. Fong and D. K. P. Ng, *J. Med. Chem.* 2011, **54**, 3097–3102.
- D. Perumal, M. Golla, K. S. Pillai, G. Raj, A. Krishna P. K. and R. Varghese, *Org. Biomol. Chem.*, 2021, **19**, 2804–2810.
- Y. Wang, M. Feng, B. Lin, X. Peng, Z. Wang, R. Lv, *Nanoscale*, 2021, **13**, 18125–18133.
- R. Lv, M. Raab, Y. Wang, J. Tian, J. Lin, P. N. Prasad, *Coord. Chem. Rev.*, 2022, **460**, 214486.
- B. Li, D. Xu, Y. Chen, W. Li, H. Liu, A. A. Ansari, R. Lv, *ACS Appl. Nano Mater.*, 2024, **7**, 9428–9440. DOI: 10.1039/D4NR01494D
- L. Feng, L. Cheng, Z. Dong, D. Tao, T. E. Barnhart, W. Cai, M. Chen and Z. Liu, *ACS Nano*, 2017, **11**, 927–937.
- X. Shi, H. Guo, X. Zhang, X. Zhang, C. Cao, H. Li, S. Chen, L. Han and S. Wang, *ACS Mater. Lett.*, 2023, **5**, 2332–2338.
- H. Tian, Z. Luo, L. Liu, M. Zheng, Z. Chen, A. Ma, R. Liang, Z. Han, C. Lu and L. Cai, *Adv. Funct. Mater.*, 2017, **27**, 1703197.
- C. McEwan, S. Kamila, J. Owen, H. Nesbitt, B. Callan, M. Borden, N. Nomikou, R. A. Hamoudi, M. A. Taylor, E. Stride, A. P. McHale and J. F. Callan, *Biomaterials*, 2016, **80**, 20–32.
- R. Zhou, T. Y. Ohulchanskyy, H. Xu, R. Ziniuk and J. Qu, *Small*, 2021, **17**, 2103569.
- H. Wang, Y. Xie, Y. Chen, H. Zhao, X. Lv, Z. Zhang, G. Li, J. Pan, J. Wang and Z. Liu, *Adv. Healthc. Mater.*, 2023, **12**, 2300848.
- S. Wang, S. Tavakoli, R. P. Parvathaneni, G. N. Nawale, O. P. Oommen, J. Hilborn and O. P. Varghese, *Biomater. Sci.*, 2022, **10**, 6399–6412.
- J. Xu, L. Xu, C. Wang, R. Yang, Q. Zhuang, X. Han, Z. Dong, W. Zhu, R. Peng and Z. Liu, *ACS Nano*, 2017, **11**, 4463–4474.
- M. Overchuk, R. A. Weersink, B. C. Wilson and G. Zheng, *ACS Nano*, 2023, **17**, 7979–8003.
- Z. Tang, Y. Liu, M. He and W. Bu, *Angew. Chem. Int. Ed.*, 2019, **58**, 946–956.
- Y. Zhou, S. Fan, L. Feng, X. Huang and X. Chen, *Adv. Mater.*, 2021, **33**, 2104223.
- Z. Yu, Y. Hu, Y. Sun and T. Sun, *Chem. Eur. J.*, 2021, **27**, 13953–13960.
- P. Zhao, H. Li and W. Bu, *Angew. Chem. Int. Ed.* 2023, **62**, e202210415.
- H. Hou, X. Huang, G. Wei, F. Xu, Y. Wang and S. Zhou, *ACS Appl. Mater. Interfaces*, 2019, **11**, 29579–29592.
- J. Qin, B. Bo, T. Yang, Z. Wang, F. Xie and H. Peng, *Mater. Lett.*, 2023, **349**, 134678.
- S. Shen, M. Liu, T. Li, S. Lin and R. Mo, *Biomater. Sci.*, 2017, **5**, 1367–1381.
- K. Li, Y. Zhang, A. Hussain, Y. Weng and Y. Huang, *ACS Biomater. Sci. Eng.*, 2021, **7**, 4420–4429.
- R. N. Woodring, E. G. Gurysh, E. M. Bachelder and K. M. Ainslie, *ACS Appl. Bio Mater.*, 2023, **6**, 934–950.
- P. Liang, B. Ballou, X. Lv, W. Si, M. P. Bruchez, W. Huang and X. Dong, *Adv. Mater.*, 2021, **33**, 2005155.
- G. Raj, V. D. S, J. Prasad, E. Anbu, S. Ram, G. B. Daniel, N. D. Narendradev, S. M. Srinivasula and R. Varghese, *Mater. Chem. Front.*, 2024, **8**, 553–561.
- A. Saminathan, J. Devany, A. T. Veetil, B. Suresh, K. S. Pillai, M. Schwake and Y. Krishnan, *Nat. Nanotechnol.*, 2021, **16**, 96–103.
- K. Dutta, R. Das, J. Medeiros and S. Thayumanavan, *Biochemistry*, 2021, **60**, 966–990.
- C. Liu, J. Hu, W. Yang, J. Shi, Y. Chen, X. Fan, W. Gao, L. Cheng, Q.-Y. Luo, M. Zhang, *Nanoscale*, 2024, **16**, 4637–4646.
- P. Borah, D. J. Baruah, P. Mridha, R. Baishya, H. K. Borab, M. R. Das, *Chem. Commun.*, 2024, **60**, 2417–2420.
- S Liu, et al., *Adv. Mater.*, 2024, **36**, 2304297.
- X. Xie, Y. Wang, X. Zhou, J. Chen, M. Wang, X. Su, *Analyst*,



- 2021, **146**, 896–903.
- 36 Q. Zhang, Q. Jiang, N. Li, L. Dai, Q. Liu, L. Song, J. Wang, Y. Li, J. Tian, B. Ding and Y. Du, *ACS Nano*, 2014, **8**, 6633–6643.
- 37 P. Pitikultham, Z. Wang, Y. Wang, Y. Shang, Q. Jiang and B. Ding, *ChemMedChem*, 2022, **17**, e202100635.
- 38 S. Dey, A. Dorey, L. Abraham, Y. Xing, I. Zhang, F. Zhang, S. Howorka and H. Yan, *Nat. Commun.*, 2022, **13**, 2271.
- 39 Y. Cao, P. Ding, L. Yang, W. Li, Y. Luo, J. Wang and R. Pei, *Chem. Sci.*, 2020, **11**, 6896–6906.
- 40 L. Fabre, C. Rousset, K. Monier, F. Da Cruz-Boisson, P. Bouvet, M.-T. Charreyre, T. Delair, E. Fleury and A. Favier, *Biomacromolecules*, 2022, **23**, 2302–2314.
- 41 W. Xuan, Y. Xia, T. Li, L. Wang, Y. Liu and W. Tan, *J. Am. Chem. Soc.*, 2020, **142**, 937–944.
- 42 C. Zhang, S. Tang, M. Wang, L. Li, J. Li, D. Wang, X. Mi, Y. Zhang, X. Tan and S. Yue, *ACS Nano*, 2024, **18**, 5470–5482.
- 43 J. He, T. Peng, Y. Peng, L. Ai, Z. Deng, X.-Q. Wang and W. Tan, *J. Am. Chem. Soc.*, 2020, **142**, 2699–2703.
- 44 A. F.-J. Jou, Y.-T. Chou, I. Willner and J. A. Ho, *Angew. Chemie Int. Ed.*, 2021, **60**, 21673–21678.
- 45 W. Xuan, Y. Xia, T. Li, L. Wang, Y. Liu and W. Tan, *J. Am. Chem. Soc.*, 2020, **142**, 937–944.
- 46 S. K. Albert, H. V. P. Thelu, M. Golla, N. Krishnan and R. Varghese, *Nanoscale*, 2017, **9**, 5425–5432.
- 47 W. Tang and S.-C. Ng, *Nat. Protoc.*, 2008, **3**, 691–697.
- 48 A. Tamura, K. Nishida, S. Zhang, T. W. Kang, A. Tonegawa and N. Yui, *ACS Biomater. Sci. Eng.*, 2022, **8**, 2463–2476.
- 49 Y. Guo, J. Zhang, F. Ding, G. Pan, J. Li, J. Feng, X. Zhu and C. Zhang, *Adv. Mater.*, 2019, **31**, 1807533.
- 50 G. Raj, D. S. Vasudev, S. Christopher, A. Babulal, P. Harsha, S. Ram, M. Tiwari, M. Sauer and R. Varghese, *Nanoscale*, 2024, **16**, 3755–3763.
- 51 N. Neelambaran, S. Shamjith, V. P. Murali, K. K. Maiti and J. Joseph, *ACS Appl. Bio Mater.*, 2023, **6**, 5776–5788.
- 52 W. Li, S. Yin, Y. Shen, H. Li, L. Yuan and X.-B. Zhang, *J. Am. Chem. Soc.*, 2023, **145**, 3736–3747.
- 53 S.-H. Park, S. Park and I. Shin, *STAR Protoc.*, 2021, **2**, 100349.
- 54 W. E. M. Noteborn, S. K. Vittala, M. B. Torredemer, C. Maity, F. Versluis, R. Eelkema and R. E. Kieltyka, *Biomacromolecules*, 2023, **24**, 377–386.
- 55 A. Rajwar, S. R. Shetty, P. Vaswani, V. Morya, A. Barai, S. Sen, M. Sonawane and D. Bhatia, *ACS Nano*, 2022, **16**, 10496–10508.
- 56 H. Naveena A and D. Bhatia, *ChemBioChem*, 2023, **n/a**, e202300506.
- 57 A. Aung, S. K. Davey, J. Theprungsirikul, V. Kumar and S. Varghese, *Adv. Healthc. Mater.*, 2023, **12**, 2201842.

View Article Online
DOI: 10.1039/D4NR01494D



Data availability statement

The data supporting this article have been included as part of the Supplementary Information

